CHEMISTRY
A EUROPEAN JOURNAL

DOI: 10.1002/chem.200601275

Hexagonal Supramolecular Architectures from Ferrocenium Cations Incorporating $[Ni(mnt)_2]^-$ Columns: Structures and Properties of [Alkylferrocene][$Ni(mnt)_2$]$^-$ Charge-Transfer Complexes (mnt = maleonitriledithiolate)

Tomoyuki Mochida,*[a, c] Takeo Koinuma,[a] Takahiro Akasaka,[a] Michiko Sato,[b] Yutaka Nishio,[b, c] Koji Kajita,[b, c] and Hatsumi Mori[d]

Abstract: The crystal architecture, magnetic properties, and thermodynamic properties of [*n*-butylferrocene][$Ni(mnt)_2$] (**1**), [*tert*-butylferrocene][$Ni(mnt)_2$] (**2**), [1,1′-diethylferrocene][$Ni(mnt)_2$] (**3**), and [1,1′-diisopropylferrocene][$Ni(mnt)_2$] (**4**) were investigated (mnt = maleonitriledithiolate). These complexes exhibit a unique supramolecular structure in which the ferrocenium cations constitute honeycomb-like assembled structures surrounding columns of the anions. For **1**, the cations form a dimer through a very short intermolecular ferrocene–ferrocene distance of 3.28 Å, which mediates an antiferromagnetic interaction with a singlet–triplet energy gap of 5 K. First-order phase transitions occur in **1**–**3** at 364, 361, and 350 K, respectively, accompanied by thermal hysteresis.

Keywords: crystal engineering · magnetic properties · metallocenes · pi interactions · self-assembly

Introduction

Crystal engineering of supramolecular organometallic materials has become an important area of research in recent years.[1–3] Among organometallic materials, metallocene-based charge-transfer (CT) complexes have attracted special attention from the viewpoint of molecular magnetism.[4] Metallocenes are also interesting in terms of phase transitions; they exhibit various transitions, such as magnetic, structural, and order–disorder transitions.[5] The $[Ni(mnt)_2]^-$ anion (mnt = maleonitriledithiolate) has frequently been used as one of the counteranions in CT complexes.[6] The anion favors one-dimensional columnar molecular arrangements, and particular arrangements of the anion engender ferromagnetic interactions.[7] Paramagnetic–diamagnetic phase transitions coupled with dimerization of anions in the column have attracted recent attention.[8] $[M(mnt)_2]^-$ (M = metal ion) anions are also used as motifs for molecular assembly.[9] A supramolecular approach to construct CT complexes is a topic with broad interest.[10] Therefore, a combination of metallocenes and $[M(mnt)_2]^-$ is interesting from the viewpoint of both crystal engineering and solid-state physical properties.

Previously, during our investigation into biferrocenium salts,[12] we discovered that a biferrocenium salt of $[Ni(mnt)_2]^-$ exhibits a spin-Peierls transition at a record high temperature of 133.2 K.[11] In this material, the valence transition of the biferrocene occurs in conjunction with the spin-Peierls transition, and is mediated by an electrostatic interaction between the iron atom of the donor (D) and the cyano group of the anion. Several intriguing $[Ni(mnt)_2]^-$ and relevant complexes that involve ferrocene-based donors are known,[13,6a] and polymorphism of $[(D)_2][\{M(mnt)_2\}_2]$ (D = $FeCp_2^*$, $CoCp_2$; Cp = ferrocene; M = Fe, Co) salts were investigated from a crystal-engineering perspective.[14] In this study, we have combined a series of alkylferrocenes with the $[Ni(mnt)_2]^-$ anion, and obtained single crystals of four charge-transfer salts: [*n*-butylferrocene][$Ni(mnt)_2$] (**1**), [*tert*-

[a] Prof. T. Mochida, T. Koinuma, T. Akasaka
Department of Chemistry, Faculty of Science
Toho University, Miyama, Funabashi, Chiba 274-8510 (Japan)
Fax: (+81) 47-472-4406
E-mail: mochida@chem.sci.toho-u.ac.jp
[b] M. Sato, Prof. Y. Nishio, Prof. K. Kajita
Department of Physics, Faculty of Science, Toho University
Miyama, Funabashi, Chiba 274–8510 (Japan)
[c] Prof. T. Mochida, Prof. Y. Nishio, Prof. K. Kajita
Research Center for Materials with Integrated Properties
Toho University, Miyama, Funabashi, Chiba 274-8510 (Japan)
[d] Prof. H. Mori
Institute for Solid State Physics, The University of Tokyo
Kashiwanoha, Kashiwa-shi, Chiba 277-8581 (Japan)

butylferrocene][Ni(mnt)$_2$] (**2**), [1,1′-diethylferrocene][Ni(mnt)$_2$] (**3**), and [1,1′-diisopropylferrocene][Ni(mnt)$_2$] (**4**). These complexes are constructed of honeycomb-like self-assembling arrangements of the donors around anion columns. A short Cp–Cp intermolecular contact was found in **1**, and the magnetic interaction mediated by the contact was evaluated by using calorimetric measurements. In addition, first-order phase transitions, which are probably correlated with intramolecular librational motion of the donors, were found above room temperature in **1**–**3**.

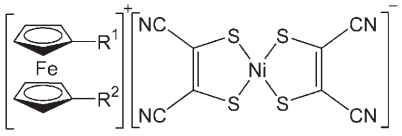

1: R^1 = *n*Bu, R^2 = H **2:** R^1 = *t*Bu, R^2 = H
3: R^1 = R^2 = Et **4:** R^1 = R^2 = *i*Pr

Results and Discussion

Preparation and general structural features: The [M(mnt)$_2$]$^-$ salts of alkylferrocenes were synthesized by means of vapor diffusion of pentane into solutions of [1,1′-dibromoferrocene][Ni(mnt)$_2$] and various alkylferrocenes dissolved in dichloromethane (Scheme 1). Single crystals were obtained for four charge-transfer salts **1**–**4**, and these were crystallographically characterized. All the salts involved ferrocenium cations and [Ni(mnt)$_2$]$^-$ monoanions, and exhibited 1:1 donor/acceptor (D/A) stoichiometry. The Fe–C(Cp) distances of the donors were within the range of 2.044(7)–2.130(2) Å, with average values of 2.076 (**1**), 2.078 (**2**), 2.093 (**3**), and 2.085 Å (**4**), which are comparable to the value for the ferrocenium cation (2.08 Å).[15] The intramolecular geometries of the anions were virtually identical to that of [NBu$_4$][Ni(mnt)$_2$],[16] with intramolecular Ni–S distances of 2.138(2)–2.155(1) Å. Infrared CN stretching bands characteristic of the monoanion were consistently observed at $\tilde{\nu}$ = 2204–2208 cm^{-1} in the IR spectra.[17]

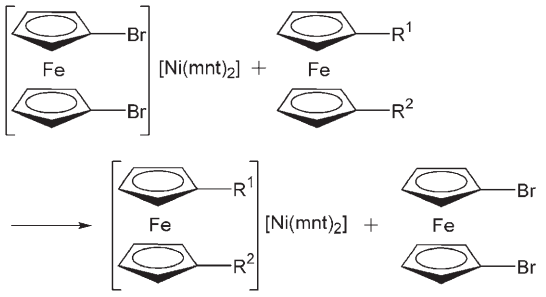

Scheme 1. General synthesis for the [alkyl ferrocene][Ni(nmt)$_2$] charge-transfer complexes.

The general structural features of **1**–**4** are described here. Interestingly, these complexes commonly exhibit segregated-stack molecular arrangements with a hexagonal assembly structure, as shown schematically in Figure 1a. The anions are stacked to form a columnar structure, and the ferrocenium cations constitute a honeycomb-type structure surrounding the anion columns. Dimensions of the hexagonal cage represented by intermolecular Fe···Fe distances (*a*, *b*, c, and *d* in Figure 1a) are listed in Table 1. The anion columns are well isolated from each other, and no direct interactions exist between the anion columns.

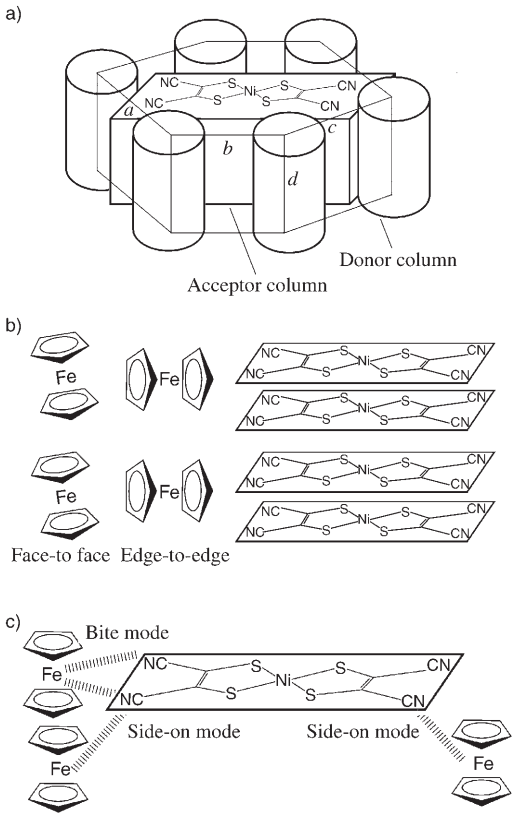

Figure 1. a) Schematic illustration of the assembled structures in **1**–**4**. b) Stacking patterns of ferrocenium cations and [Ni(mnt)$_2$]$^-$ anions, which exhibit the same stacking periodicity. c) Fe···NC– interaction modes between the donor and acceptor.

Table 1. Intermolecular Fe···Fe distances [Å] in **1**–**4** for the hexagonal units shown in Figure 1a.

Compound	*a*	*b*	*c*	*d*
1	6.711	7.173	11.621	7.029
2 (unit A)	6.614	7.856	11.741	7.094, 7.480
(unit B)	6.629	7.354	12.217	7.094, 7.480
3	8.177	8.177	8.404	7.223
4	7.461	9.034	9.661	8.187

In general, [metallocene][metal–dithiolene] charge-transfer complexes tend to give mixed-stack structures.[6a,13a] Therefore, the present structure is unique and interesting from a crystal-engineering perspective. As shown in this study, this architecture is one of the general structural types for metallocenium complexes, and is also observed for $[(D)_2][\{M(mnt)_2\}_2]$ ($D = FeCp_2^*$, $CoCp_2$),[14] and ferrocenium salts with 7,7,8,8-tetracyano-*p*-quinodimethane (TCNQ) derivatives.[18] All these materials are 1:1 D/A salts in which each component forms a columnar structure. The generality of the hexagonal supramolecular structure is a consequence of the inherent intermolecular forces of each component, the stacking tendency of the acceptor, the flexible packing tendency of ferrocenes, and their molecular shapes. Owing to their nonplanarity and nonspecific intermolecular interactions, ferrocenes can assume face-to-face, edge-to-edge, and also intermediate stacking patterns (Figure 1b), while maintaining a similar stacking periodicity. The in-plane D/A ratio required for the hexagonal structure is 2:1, and this is balanced by the 1:2 D/A ratio along the stacking direction within each column; the packing periodicity of ferrocenes is twice that of the acceptor along the stacking direction, as shown in Figure 1b. It is important that the molecular sizes of the donor and the acceptor are comparable. The calculated molecular volume of $[Ni(mnt)_2]^-$ in the crystal was 231 Å^3, and those for the ferrocenium cations were 231 (*n*-butylferrocene), 230 (*tert*-butylferrocene), 234 (1, 1′-diethylferrocene), and 266 Å^3 (1,1′-diisopropylferrocene). No crystalline salts could be obtained for other substituted ferrocenes (see the Experimental Section), and this is possibly as a result of a mismatch of the molecular volume. The hexagonal assembly, accounted for by the geometric factors, is a result of nonspecific self-assembly of the donor and acceptor columns that probably minimizes electrostatic interactions, although there may be stabilization caused by some local donor–acceptor interactions. The hexagonal assembly is also generally seen in molecular assemblies composed of rod-shaped or round-shaped molecules in various phases. Some metal–organic composites exhibit honeycomb or hexagonal structures, which are organized by means of coordination bonding.[1–3] It is interesting that such a structure was formed in these ionic molecular materials without using specific interactions.

The local structures between the donor columns and acceptor columns were also examined. In all the complexes, every Fe atom of the donor is surrounded by three or four cyano groups of the acceptor. This type of arrangement is also observed in [biferrocene][$Ni(mnt)_2$]$^-$ salts.[11] The Fe···N distances were found to be 4.13–4.63 Å and longer than the sum of the van der Waals distances, but the arrangement may have occurred for steric or electrostatic reasons, and may be significant considering the frequent occurrence of the arrangement. Figure 1c schematically illustrates the two types of donor–acceptor arrangements found in these complexes: the bite mode and the side-on mode. Both modes are observed in **2** and **3**, in which the ferrocenium cations (Cp planes) are nearly parallel to the molecular planes of the anions. However, in **1** and **4** the ferrocenium cations are aligned almost perpendicular to the acceptors, so that the anions cannot chelate to the Fe atom and only the side-on mode is observed.

Acceptor arrangements: The acceptors in **1**–**4** exhibit a columnar arrangement of the dimerized anions with parallel molecular axes. The arrangements of the acceptors are shown in Figure 2. Selected intra- and interdimer distances

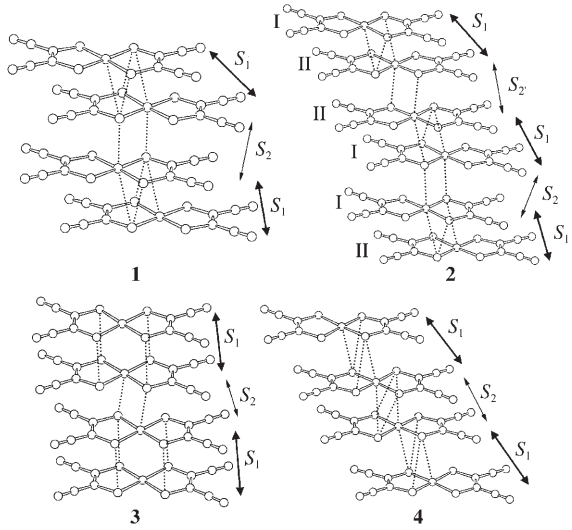

Figure 2. Arrangements of $[Ni(mnt)_2]^-$ anions in **1**, **2**, **3**, and **4**. Dashed lines indicate short intermolecular S···S and S···Ni distances. S_1 indicates an intradimer interaction and S_2 indicates an interdimer interaction.

are listed in Table 2. To estimate the degree of intermolecular interaction, the overlap integrals between the LUMO of the acceptors were calculated and are listed in Table 2. Figure 2 shows the intra- and interdimer interactions that correspond to the overlap integrals S_1 and S_2, respectively. There are two interdimer interactions for **2**, S_2 and $S_{2'}$, because the complex has two crystallographically independent anions (anions I and II). Within the dimer, S···S distances shorter than the sum of the van der Waals distances (3.7 Å) are found, apart from in **4**. There were no contact distances between the dimers in any of the salts. In particular, the anions in **3** interact strongly in the dimer in a face-to-face manner with short intradimer S···S distances of 3.43 and 3.54 Å. The dimers in the other complexes are in slipped conformations that give weaker intradimer interactions. Correspondingly, the intradimer overlap integral in **3** was exceptionally large (35×10^{-3}), whereas those for **1** and **2** were 18×10^{-3}, and that for **4** was 12×10^{-3}. The structure of **3** was also determined at high temperature (see below), and the same tendency was confirmed. Overall, the degree of dimerization is strong. S_1/S_2 in **1** was 18, which is very large and for **2**–**4** ranged from 3 to 7. With regards to the Ni···Ni distances, the intradimer distance (3.5 Å) in **3** is shorter than the interdimer one (3.7 Å), but in the other complexes, the

Table 2. Intra- and interdimer distances [Å] and overlap integrals *S* for **1**–**4**.

Compound		S···S[a]	Ni···S[a]	Ni···Ni	Interplane dist.[c]	$S^{[d]}/10^{-3}$
1	(intradimer)	3.575	3.565	4.311	3.355	18.1
	(interdimer)	3.829[b]	3.643	3.910	3.588	1.2
2	(intradimer)	3.574	3.584	4.338	3.393	18.6
	(interdimer)	3.748,[b,e] 3.747[b,f]	3.437,[e] 3.545[f]	3.824,[e] 3.802[f]	3.477,[e] 3.461[f]	6.0,[e] 2.7[f]
3 (150 K)	(intradimer)	3.434	4.049	3.514	3.480	35.1
	(interdimer)	3.766[b]	3.608	3.788	3.556	9.1
3 (343 K; RT phase)	(intradimer)	3.492	4.088	3.545	3.538	35.3
	(interdimer)	3.811[b]	3.770	3.841	3.639	13.0
3 (343 K; HT phase)	(intradimer)	3.564	3.912	3.626	3.541	26.2
	(interdimer)	3.832[b]	3.758	3.851	3.635	6.7
4	(intradimer)	3.838[b]	3.586	4.438	3.433	12.5
	(interdimer)	3.873[b]	3.833	4.018	3.619	4.1

[a] The shortest distances. [b] Distances longer than the van der Waals distances (3.7 Å). [c] Distances between the coordination planes. [d] Overlap integrals calculated by the EHMO method. [e] Between molecules I–I. [f] Between molecules II–II.

intradimer Ni···Ni distances (4.3–4.4 Å) are longer than the interdimer ones (3.8–4.0 Å). All the complexes were electrically insulating, which is consistent with these structural features.

Crystal structures: A packing diagram of **1**, viewed along the stacking axis (*a* axis), is shown in Figure 3. The anion columns are surrounded by six cations. The unit cell contains one crystallographically independent molecule of each component. The ferrocenium cations (Cp planes) are almost perpendicular to the acceptors, and are stacked in an edge-to-edge manner. The donor molecules form a dimer through π–π interactions between the Cp rings. The intermolecular distances between the Cp rings in the dimer are unusually short, with an interplane distance of 3.282 Å and a centroid–centroid distance of 3.317 Å. These are much shorter than the usual π–π intermolecular distance of 3.4–3.6 Å. The intermolecular Fe···Fe distance in the dimer is 6.71 Å. A search of the Cambridge Structural Database (CSD version 5.27, 2005) revealed that the intermolecular Cp–Cp distance in **1** is the shortest reported to date for ferrocene-related complexes. Only a few ferrocenium complexes exhibit intermolecular Cp–Cp (centroid) distances shorter than 3.4 Å. Distances of 3.33–3.38 Å were found in ferrocenium iodide derivatives[19] and for a ferrocenium salt of $[Ni(mnt)_2]^-$.[13d] Complexes **2**–**4** did not display such short intermolecular Cp–Cp contacts. The Cp–Cp contact in **1** causes antiferromagnetic interactions within the dimer (see below). Figure 3 also shows the Fe···NC– distances between the donors and the anions (4.27, 4.29, 4.31 Å). Each Fe atom is surrounded by three cyano groups. Of the four cyano groups of $[Ni(mnt)_2]^-$, two at opposite positions are located near the Fe atom in the side-on mode, and two of the six ferrocene molecules in the hexagon interact with the $[Ni(mnt)_2]^-$ column at the center.

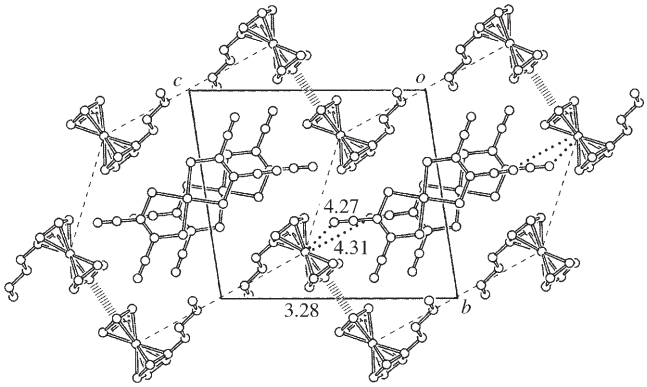

Figure 3. Packing diagrams of **1** viewed along the *a* axis. Dashed lines connecting the Fe atoms of the donors are only drawn as geometric indicators. Fe···NC– intermolecular distances (<4.7 Å) are shown by dotted lines. Thick broken lines represent close contacts between the Cp rings. Hydrogen atoms are omitted for clarity. All distances are given in Å.

A packing diagram of **2** viewed along the stacking axis (*b* axis) is shown in Figure 4. The unit cell contains two crystallographically independent molecules of each component. The donor molecules are stacked at an angle along the *b* axis. Each Fe atom is surrounded by three cyano groups. The Fe···NC– distances between the donors and the anions, 4.13–4.63 Å (bite mode) and 4.18–4.50 Å (side-on mode), are complicated and not shown in Figure 4. For anion I, two

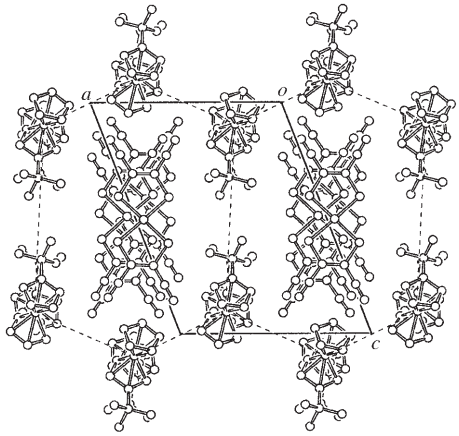

Figure 4. Packing diagram of **2** viewed along the *b* axis. Dashed lines connecting the Fe atoms of the donors are only drawn as geometric indicators. Hydrogen atoms are omitted for clarity.

cyano groups are located near the Fe atoms and the other two cyano groups are free, whereas only one cyano group is free for anion II. All six ferrocene molecules in the hexagon interact with the $[Ni(mnt)_2]^-$ column at the center.

A packing diagram of **3** at 150 K viewed along the *a* axis is shown in Figure 5. The unit cell contains one crystallographically independent molecule of each component. The

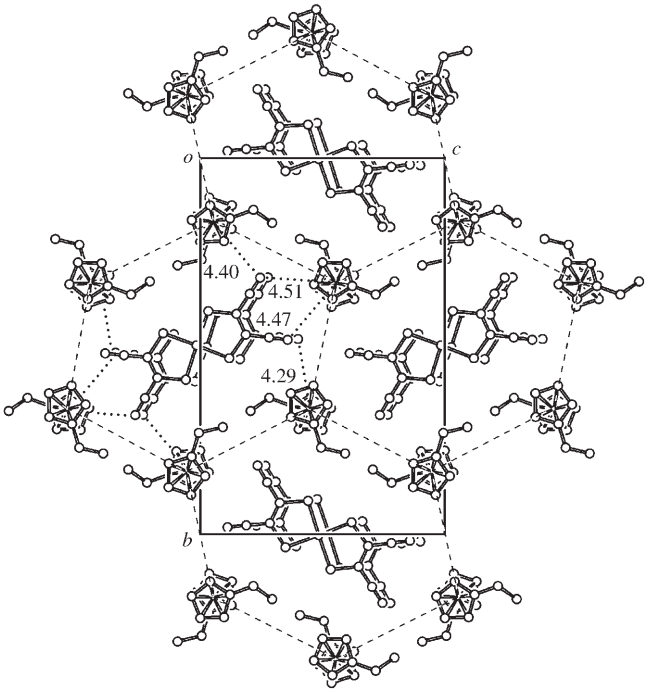

Figure 5. Packing diagram of **3** viewed along the *a* axis. Dashed lines connecting the Fe atoms of the donors are only drawn as geometric indicators. Fe···NC− intermolecular distances (<4.7 Å) are shown by dotted lines. Hydrogen atoms are omitted for clarity. All distances are given in Å.

donors almost stack in a face-to-face manner but π–π interactions between the donors are small, with a Cp–Cp distance of 3.881 Å (centroid–centroid). Each Fe atom is surrounded by four cyano groups. Two of the four cyano groups of the anion are located near the Fe atom. The Fe···N distances are 4.47 and 4.51 Å (bite mode) and 4.29 and 4.40 Å (side-on mode). Thus, all six ferrocene molecules in the hexagon interact with $[Ni(mnt)_2]^-$ at the center. The structure of **3** was further examined at 343 K, in connection with the first-order phase transition above room temperature (see below).

A packing diagram of **4** viewed along the stacking axis (*b* axis) is shown in Figure 6. The unit cell contains one crystallographically independent molecule of each component. The donors stack in an edge-to-edge manner and no π–π interactions are present. The Cp planes of the ferrocenium cations are almost perpendicular to the acceptors. Each Fe atom is surrounded by four cyano groups. Of the four cyano groups in the anion, three are located near the Fe atoms in the side-on mode (Fe···N distances are 4.00, 4.48, and 4.61 Å),

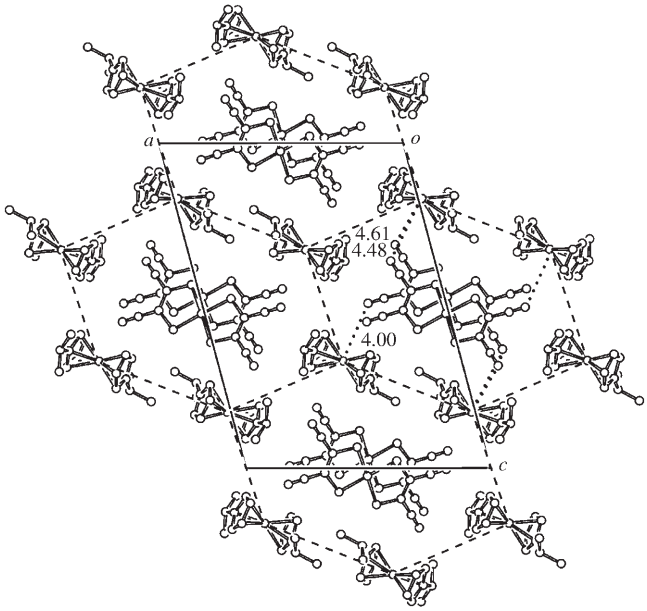

Figure 6. Packing diagram of **4** viewed along the *b* axis. Dashed lines connecting the Fe atoms of the donors are only drawn as geometric indicators. Fe···NC− intermolecular distances (<4.7 Å) are shown by dotted lines. Hydrogen atoms are omitted for clarity. All distances are given in Å.

and four of the six ferrocene molecules in the hexagon interact with $[Ni(mnt)_2]^-$ at the center.

Magnetic susceptibilities: The magnetic susceptibilities of complexes **1**–**4** are shown in Figure 7 in the form of χT–T plots. The χT values are almost temperature independent,

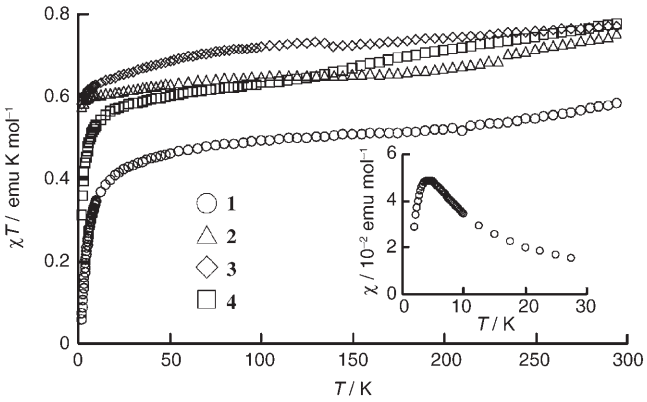

Figure 7. Temperature dependence of the magnetic susceptibilities of **1**–**4** represented in the form of χT versus T. The inset shows the χ versus T plot for **1**.

which indicates that these complexes are paramagnetic. The magnetic susceptibilities are dominated by the contribution of the donor spins because the $[Ni(mnt)_2]^-$ anions form columns with strong dimerization. χT values of approximately 0.6 emu K mol^{-1} are reasonable for the ferrocenium cations, which are larger than the spin-only values as a consequence

of orbital contribution.[20] Variation in the molar magnetic susceptibilities at room temperature is attributed to the orientation effect associated with the large magnetic anisotropy of the ferrocenium cation.[21] Another possibility for the lower χT value in **1** may be a partial loss of orbital contribution. A slight enhancement of the magnetic susceptibilities above 200 K was observed for **1** and **2**, and is possibly a result of thermal activation of the anion spins.

The consequence of the dimerization of the cations in **1** was observed in its magnetic properties. The inset diagram in Figure 7 shows the χ–T plot of **1** with a maximum at approximately 4.2 K; below this temperature χ decreased. No other complex exhibited a decrease in χ within the measured temperature range. A decrease in the χT value was observed in the low-temperature region for **1** and **4**, and their susceptibilities were analyzed based on the Curie–Weiss law. The parameters obtained for **1** extrapolated from the data measured between 5–15 K were $C = 0.56$ emu K mol^{-1} and $\theta = -6.17$ K, in which C is the Curie constant and θ is the Weiss temperature. The values obtained for **4** by using the data between 2–15 K were $C = 0.62$ emu K mol^{-1} and $\theta = -1.73$ K. Although the Fe···Fe distances in **2** (6.614 and 6.629 Å) are shorter than that in the dimer of **1** (6.71 Å), **2** exhibited no magnetic interaction at low temperatures. This observation also supports the fact that the Cp–Cp contact in **1** provides the interaction pathway.

For the thermodynamic characterization of the magnetic interaction in **1**, the heat capacity was measured for single crystals. Figure 8 shows the excess molar heat capacity for **1** below 8 K, which was obtained by subtracting the lattice contribution. An excess heat capacity reminiscent of a Schottky anomaly was observed, which exhibits a maximum at approximately 2 K (at $H = 0$ T). This behavior is attributed to local magnetic ordering within the dimer of the ferrocenium cations in **1**. Application of external magnetic fields induced a low-temperature shift of the anomaly, which confirmed the antiferromagnetic interaction. The resulting excess entropy (ΔS), estimated by integration of the excess term, was close to $R\ln 2$ ($= 5.76$ J mol^{-1} K^{-1}). This result indicates that the magnetic interaction occurs between $s = 1/2$ spins, which suggests that the orbital contribution has disappeared above this temperature region. The excess heat capacity (C_M) was analyzed based on a singlet–triplet model ($H = -2Js_1 \cdot s_2$) within the dimer, according to Equation (1):

$$C_M = Nk_B\beta^2\{(2J-h)^2\exp[-\beta(2J-h)] + (2J)^2\exp(-2\beta J) + (2J+h)^2\exp[-\beta(2J+h)] + h^2\exp[-\beta(4J-h)] + h^2\exp[-\beta(4J+h)] + 4h^2\exp(-4\beta J)\}/Z^2 \quad (1)$$

$$Z = 1 + \exp(-2\beta J) + \exp[-\beta(2J-h)] + \exp[-\beta(2J+h)],$$
$$h = g\mu_B H, \qquad \beta = 1/k_B T$$

in which g, μ, H, and k_B are the g factor, Bohr magnetron, external magnetic field, and the Boltzmann constant, respectively. The analysis reproduced the heat capacity reasonably, in addition to its field dependence (Figure 8b), and allowed

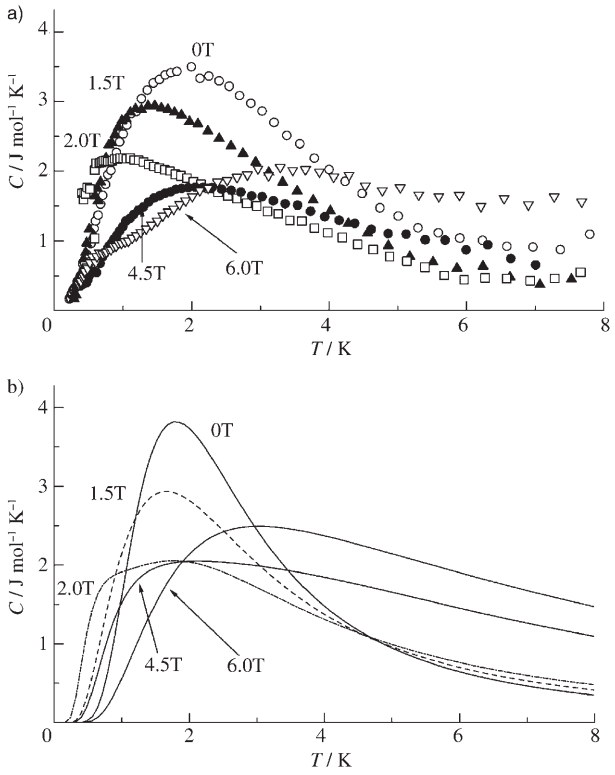

Figure 8. Temperature dependence of the excess heat capacity of **1** under various magnetic fields. a) Experimental data. b) Theoretical fit based on a singlet–triplet model with $2J = -5$ K.

the singlet–triplet energy gap ($|2J|$) value of 5 K to be determined. The broadness of the experimental curves compared with the simulated one is attributed to the presence of a weak interaction between the dimers that was not taken into account in the analysis. We have shown that the interaction could be evaluated by calorimetric measurements, whereas the analysis of magnetic behaviors of the ferrocenium salts at low temperature becomes somewhat obscure as a result of orbital contributions. Furthermore, direct intermolecular magnetic interactions between ferrocenium cations, if any, are usually negligible or smaller than a few kelvin owing to bulkiness and a nonspecific packing tendency.[13,19,22] However, we could observe the magnetic interaction between the cations with short intermolecular Cp–Cp contacts.

First-order phase transitions at high temperature: First-order phase transitions, above room temperature, were found for **1**–**3** by using differential scanning calorimetry (DSC). The thermodynamic data are summarized in Table 3. The DSC curve of **3** is shown in Figure 9 for two successive runs, in which endothermic peaks are displayed at approximately 77 °C (350 K) on heating and exothermic peaks at approximately 58 °C (331 K) on cooling. The transition accompanies a hysteresis of 19 K. Each peak is composed of several small peaks, which is probably a consequence of the size dependence of the phase transition.[5] Increasing the

Table 3. DSC data for the phase transitions of **1–3**.

Compound	Heating run			Cooling run			ΔT
	T_C [K]	ΔH [kJ mol^{-1}]	ΔS [J K^{-1} mol^{-1}]	T_C [K]	ΔH [kJ mol^{-1}]	ΔS [J K^{-1} mol^{-1}]	[K]
1	363.9	5.23	14.4	312.4	4.53	14.4	51.5
2	361.7	3.31	9.1	353.4	2.39	6.8	8.3
3	350.3	4.99	14.3	330.6	3.80	11.5	19.7

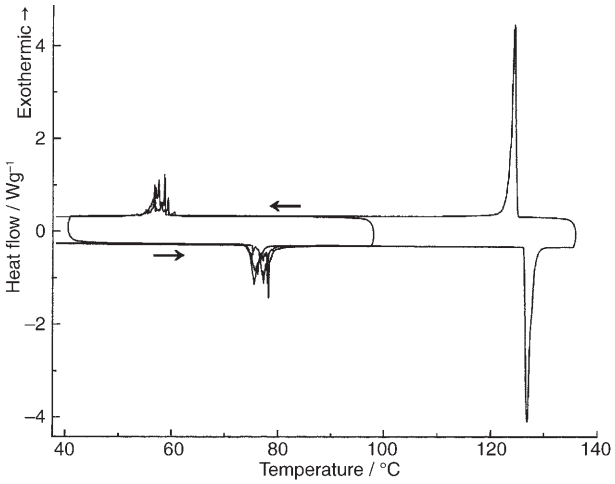

Figure 9. DSC curves for **3**.

temperature resulted in the observation of a melting peak at 398.1 K ($\Delta H_{melt}=16$ kJ mol^{-1}, $\Delta S_{melt}=40$ J K^{-1} mol^{-1}). Complexes **1** and **2** exhibited similar transitional behavior, but no melting peaks were observed up to 450 K. The transition temperatures were 364 K for **1** and 362 K for **2** during the heating process, accompanied by hystereses of 52 and 8 K, respectively. No such phase transitions were observed for **4**; it decomposed after melting at $T_C=440.8$ K ($\Delta H_{melt}=27$ kJ mol^{-1}, $\Delta S_{melt}=62$ J K^{-1} mol^{-1}; T_C = Curie temperature). The entropy change of the transitions observed for **1–3** are in the order of 10 J K^{-1} mol^{-1}, which suggests the occurrence of order–disorder or dynamic phenomenon in the crystal. At high temperatures metallocenes often undergo order–disorder transitions associated with molecular motion, and in some cases they change into plastic phases.[5] The small entropy changes in **1–3** indicate that their transitions do not result in plastic phases. This supposition was also supported by crystallographic data for **3**, as described below.

For the structural characterization of the phase transition, the crystal structure of **3** was analyzed for both phases. The structures were compared at the same temperature (343 K) in the same crystal, by taking advantage of the hysteresis (Figure 9). When the crystal temperature was raised from room temperature (RT) to 343 K, the RT-phase data were collected. The temperature was then raised to 363 K and gradually cooled to 343 K, and high temperature (HT)-phase data were collected.

The cell parameters of **3** under three different conditions are shown in Table 4. The packing structures and space group are essentially unchanged, but the cell parameters show slight differences. At the same temperature (343 K), the RT unit cell ($V=2419.6(8)$ Å^3) is smaller than the HT unit cell ($V=2452.3(6)$ Å^3), and is accompanied by a decrease in density (ρ_{calcd}) from 1.596 to 1.545 g cm^{-3}. The packing coefficients calculated from the structures are 0.68 (HT Phase) and 0.69 (RT phase), whereas the value is 0.72

Table 4. Crystallographic parameters for **1–4**.

	1	**2**	**3** (150 K)	**3** (343 K; RT phase)	**3** (343 K; HT phase)	**4**
empirical formula	$C_{22}H_{18}FeN_4NiS_4$	$C_{22}H_{18}FeN_4NiS_4$	$C_{22}H_{18}FeN_4NiS_4$	$C_{22}H_{18}FeN_4NiS_4$	$C_{22}H_{18}FeN_4NiS_4$	$C_{24}H_{22}FeN_4NiS_4$
formula weight	581.2	581.2	581.2	581.2	581.2	609.3
crystal dimensions [mm^3]	0.40×0.40×0.30	0.50×0.20×0.13	0.68×0.13×0.13	0.68×0.13×0.13	0.68×0.13×0.13	0.47×0.13×0.13
crystal system	triclinic	triclinic	monoclinic	monoclinic	monoclinic	monoclinic
a [Å]	7.0295(4)	12.3294(7)	7.2228(15)	7.3032(13)	7.4050(11)	15.4874(10)
b [Å]	12.3646(8)	14.5679(8)	22.394(4)	22.597(4)	22.880(4)	8.1869(5)
c [Å]	14.0343(9)	15.7742(9)	14.587(3)	14.716(3)	14.592(2)	21.3791(14)
α [°]	98.412(1)	104.314(1)	–	–	–	–
β [°]	107.070(2)	104.704(1)	95.301(3)	94.970(4)	97.318(4)	104.9280(10)
γ [°]	90.261(1)	107.866(1)	–	–	–	–
V [Å^3]	1193.98(13)	2440.3(2)	2349.3(8)	2419.6(8)	2452.3(6)	2619.3(3)
space group	$P\bar{1}$	$P\bar{1}$	$P2_1/c$	$P2_1/c$	$P2_1/c$	$P2_1/n$
Z value	2	4	4	4	4	4
ρ_{calcd} [g cm^{-3}]	1.617	1.582	1.643	1.596	1.574	1.545
$F(000)$	592	1184	1184	1184	1184	1248
no. of reflections	8899	18188	13254	17716	17978	18541
no. of observations	5859	11964	5633	6024	6089	6510
parameters	290	583	291	291	291	291
T [K]	173	173	150	343	343	173
R_1, R_w ($I>2\sigma$)	0.0317, 0.0776	0.0775, 0.1378	0.0606, 0.1103	0.0646, 0.1410	0.0767, 0.2365	0.0377, 0.0806
R_1, R_w (all data)	0.0428, 0.0836	0.0916, 0.1433	0.1241, 0.1301	0.1928, 0.1886	0.2033, 0.2975	0.0640, 0.0914
goodness of fit	1.046	1.020	1.032	0.949	0.999	0.994

at 150 K. The angle β displays the most significant difference of the cell parameters for the three conditions. The β value (94.970(4)°) of the RT phase at 343 K is slightly smaller than that at 150 K (95.301(3)°), but the value is larger for the HT phase at 343 K (97.318(4)°). The relative arrangement of the donor and acceptor is slightly different in the unit cell. The molecular structures are almost the same for both phases, but the thermal ellipsoids of the donor, and in particular, those of the alkyl moieties, are larger in the HT phase than in the RT phase, whereas those of the acceptor are not as large. This result suggests that the phase transition is probably associated with an intramolecular librational or rotational motion of the substituents or rings of the donors, although such disorder could not be resolved. This observation is consistent with the absence of such a transition in **4**, which has the donor with the bulkiest substituent and its molecular shape is the least symmetric. On the other hand, the acceptors are strongly dimerized, even in the HT phase. The phase transition is not correlated with a change in the anion arrangement, such as dimer–nondimer (diamagnetic–paramagnetic) phase transitions[8] exhibited by some $[Ni(mnt)_2]^-$ salts. The intermolecular distances and overlap integrals between the anions are shown in Table 2. Comparison of the RT-phase structures at 150 and 343 K showed that the intermolecular distances are slightly longer at 343 K, but the overlap integrals are comparable. On the other hand, comparison of the RT and HT structures at 343 K shows that the intermolecular distances are longer in the latter, and more significantly, both the intradimer and interdimer overlap integrals are smaller for the HT phase than for the RT phase by approximately 25%. For the magnetic measurement, an increase of χT by approximately 7% was observed at the transition temperature, which probably corresponds to a weakening of the interaction between the anion spins. High-temperature structures of other complexes could not be determined owing to instrumental limitations. The packing coefficients for **1**, **2**, and **4** at 153–170 K were 0.70, 0.69, and 0.69, respectively. Although many metallocene-related compounds exhibit order–disorder phase transitions at high temperatures, it is interesting that such transitions were found in the highly organized charge-transfer complexes of **1**–**3**.

Conclusion

We have prepared four [alkylferrocene][$Ni(mnt)_2$] complexes and investigated their structures and magnetic properties. All complexes were ferrocenium salts with 1:1 D/A stoichiometry. These complexes formed honeycomb-like supramolecular structures, which involved hexagonal arrangements of the donors around the acceptor columns. The assembled structure may be interesting from a crystal-engineering perspective because the structures result from characteristic packing tendencies, molecular shapes, and volumes of the ferrocene molecules and $[Ni(mnt)_2]^-$. Hexagonal assemblies are generally observed in a molecular assembly composed of rod-shaped or round-shaped molecules without specific interactions in various phases, such as interfaces, and honeycomb structures are often seen in ionic materials or metal–organic hybrids with assemblies that are specifically directed by coordination bonds. However, the supramolecular formation observed in this work is not a result of specific intermolecular interactions, but rather a result of self-assembly. It is interesting that such a hexagonal structure was constructed in ionic molecular materials. With regards to the physical properties, $[Ni(mnt)_2]^-$ anions in these complexes were strongly dimerized and no spin-Peierls-like transitions were observed. However, first-order phase transitions were found in three complexes above room temperature; these transitions accompany thermal hystereses of 8–52 K and entropy changes in the order of $10\,J\,K^{-1}\,mol^{-1}$ and are probably associated with intramolecular librational motion of the donors. An unusually short intermolecular Cp–Cp contact (centroid–centroid distance: 3.317 Å) was found in the *n*-butylferrocenium salt, from which a dimer of the ferrocenium cation was formed. To the best of our knowledge, this is the shortest distance in a ferrocenium-related salt reported to date. Usually, direct intermolecular magnetic interactions between ferrocenium cations are negligibly small. However, an antiferromagnetic interaction resulting from the short Cp–Cp contact was observed here, and the singlet–triplet gap (5 K) was evaluated by using calorimetry. In this study, we have shown that the combination of ferrocene and $[Ni(mnt)_2]^-$ yields CT complexes that are interesting from aspects of both crystal engineering and solid-state physical properties. We have prepared ferrocenium salts with TCNQ derivatives,[18] which are closely related materials, and their structures and physical properties will be reported elsewhere.

Experimental Section

General: $[NBu_4][Ni^{III}(mnt)_2]$ and substituted ferrocenes were purchased from TCI. Infrared spectra were recorded on an FTIR 230 spectrometer (JASCO) as KBr pellets in the $\tilde{\nu} = 4000$–$400\,cm^{-1}$ range. Magnetic susceptibilities were measured by using a MPMS-2 SQUID susceptometer (Quantum Design) in the temperature range of 2–300 K at a constant field of 5000 G. The diamagnetic contribution to the magnetic susceptibility of $[Ni(mnt)_2]^-$ was taken from the literature,[7c] and those of the ferrocene molecules were calculated by using Pascal's law. DSC measurements were performed by using a Q100 differential scanning calorimeter (TA instruments) in the temperature range 100–450 K at a rate of $10\,K\,min^{-1}$. The thermodynamic data were averaged over a few cycles. Specific heat data for single crystals of **4** (ca. 0.3 mg) were measured by using the thermal relaxation method in the temperature range of 0.2–8 K. Stainless steel wires with a diameter of 15 μm were used for both the electrical leads and thermal contact leads between the sample and the thermal bath. The temperature of the thermal bath and the samples were measured by using a Cernox 1010 resistance thermometer. Intermolecular overlap integrals were calculated by using the extended Hückel molecular orbital (EHMO) method using a software package developed by Professor Takehiko Mori (Tokyo Institute of Technology).[23] Molecular volumes and packing coefficients were calculated with Spartan '04[24] and PLATON,[25] respectively, using crystallographic data.

X-ray structure analysis: X-ray diffraction data for single crystals were collected on a Bruker SMART APEX CCD diffractometer, by using

$Mo_{K\alpha}$ radiation ($\lambda = 0.71073$ Å). Crystal data, data collection parameters, and analysis statistics for these compounds are listed in Table 4. All calculations were performed by using SHELXL.[26] The non-hydrogen atoms were anisotropically refined, and hydrogen atoms were inserted at calculated positions. Empirical absorption corrections were applied. The packing diagrams were drawn by using ORTEP-3.[27] CCDC-297334 (**1**), -297335 (**2**), -297336 (**3**), -618089 (**3**, at 343 K, RT phase), -618090 (**3**, at 343 K, HT phase), and -297337 (**4**) contain the supplementary crystallographic data for this paper. These data can be obtained free of charge from the Cambridge Crystallographic Data Centre via www.ccdc.cam.ac.uk/data_request/cif.

Preparation of 1,1′-dibromoferrocenium hexafluorophosphate: 1,1′-Dibromoferrocene (100 mg, 0.29 mmol) was dissolved in concentrated sulfuric acid (1.5 mL), and the solution was stirred for 4 h at room temperature. The solution was cooled in an ice bath, and water (1.5 mL) was added portionwise before it was filtered through a glass filter. The filtrate was added to an aqueous solution (0.5 mL) of NH_4PF_6 (151 mg, 0.926 mmol). Dark blue powders precipitated, were collected by filtration, and were then washed successively with water, ethanol, and hexane before they were vacuum dried (73.4 mg, 51.6 %). FTIR (KBr): $\tilde{\nu} = 1416$, 836, 557 cm^{-1}.

Preparation of [1,1′-dibromoferrocene][Ni(mnt)$_2$]: Solutions of $[NBu_4][Ni^{III}(mnt)_2]$ (50 mg, 0.1023 mmol) and 1,1′-dibromoferrocenium hexafluorophosphate (29.7 mg, 0.05107 mmol) in 1,2-dichloroethane (2.5 mL) were prepared and slowly mixed after filtration. The solution was carefully concentrated with gentle heating, and allowed to cool to room temperature. Black needle-like crystals formed within a few days (20.5 mg, 58.8 %). FTIR (KBr): $\tilde{\nu} = 2204$, 1413 cm^{-1}.

Preparation of charge-transfer complexes: A solution of [1,1′-dibromoferrocene][Ni(mnt)$_2$] (5 mg, 7.32 mmol) in CH_2Cl_2/acetone (2 mL) and a solution of alkylferrocene (7.32 mmol) in CH_2Cl_2 (2 mL) were mixed, and pentane vapor was diffused into this solution at room temperature under a nitrogen atmosphere. Black needle-like crystals of a charge-transfer complex formed within a few days with a yield of approximately 50 %. Crystal growth of **4** often required a longer period of time and the yield was sometimes poor. Other substituted ferrocenes (di-*n*-butyl-, dimethyl-, ethyl-, *tert*-pentyl-, cyclohexenyl-, cyclopentenyl-, vinyl-, and ethynyl- derivatives) did not afford crystalline products.

Complex ***1***: IR (KBr): $\tilde{\nu} = 2204$, 1417 cm^{-1}; elemental analysis calcd (%) for $C_{22}H_{18}FeN_4NiS_4$: C 45.46, H 3.12, N 9.64; found: C 45.20, H 3.19, N 9.64.

Complex ***2***: IR (KBr): $\tilde{\nu} = 2205$, 1417 cm^{-1}; elemental analysis calcd (%) for $C_{22}H_{18}FeN_4NiS_4$: C 45.46, H 3.12, N 9.64; found: C 44.97, H 3.30, N 9.23.

Complex ***3***: IR (KBr): $\tilde{\nu} = 2204$, 1427 cm^{-1}; elemental analysis calcd (%) for $C_{22}H_{18}FeN_4NiS_4$: C 45.46, H 3.12, N 9.64; found: C 44.80, H 3.17, N 9.44.

Complex ***4***: IR (KBr): $\tilde{\nu} = 2208$, 1418 cm^{-1}; elemental analysis calcd (%) for $C_{24}H_{22}FeN_4NiS_4$: C 47.31, H 3.64, N 9.20; found: C 46.96, H 3.75, N 9.15.

Acknowledgements

This work was financially supported by a Grant-in-Aid for Scientific Research (no. 17685003) from the Japan Society for the Promotion of Science (JSPS) and the "High-Tech Research Center" Project 2005–2009 from the Ministry of Education, Culture, Sports, Science, and Technology of Japan (MEXT). We thank Dr. Katsuyoshi Mitsunaga (School of Pharmaceutical Sciences, Toho University) for performing the elemental analyses. We also thank Mr. Masaru Nakama (WarpStream, Tokyo) for providing the Web-DB computer systems. This work was performed by using the facilities of the Institute for Solid State Physics, the University of Tokyo.

[1] a) *Comprehensive Supramolecular Chemistry, Vol. 1–11* (Eds.: J.-M. Lehn, J. L. Atwood, J. E. D. Davis, D. D. MacNicol, F. Vögtle), Pergamon Press, Oxford, **1990–1996**; b) J.-M. Lehn, *Supramolecular Chemistry, Concepts and Perspectives*, VCH, Weinheim, **1995**; c) C. Janiak, *Dalton Trans.* **2003**, 2781; d) P. D. Beer, P. A. Gale, G. Z. Chen, *J. Chem. Soc., Dalton Trans.* **1999**, 1897.

[2] a) D. Braga, F. Grepioni, G. R. Desiraju, *Chem. Rev.* **1998**, *98*, 1375; b) D. Braga, L. Brammer, N. R. Champness, *CrystEngComm* **2005**, *7*, 1; c) *The Crystal as a Supramolecular Entity (Perspect. Supramol. Chem., Vol. 2)*, (Ed.: G. R. Desiraju), Wiley, Chichester, **1996**.

[3] a) R. Horikoshi, C. Nambu, T. Mochida, *New J. Chem.* **2004**, *28*, 26; b) R. Horikoshi, M. Ueda, T. Mochida, *New J. Chem.* **2003**, *27*, 933; c) R. Horikoshi, C. Nambu, T. Mochida, *Inorg. Chem.* **2003**, *42*, 6868; d) R. Horikoshi, T. Mochida, H. Moriyama, *Inorg. Chem.* **2002**, *41*, 3017; e) T. Mochida, K. Okazawa, R. Horikoshi, *Dalton. Trans.* **2006**, 693.

[4] a) J. S. Miller, A. J. Epstein, W. M. Reiff, *Angew. Chem.* **1994**, *106*, 399; *Angew. Chem. Int. Ed. Engl.* **1994**, *33*, 385, and references therein; b) *Ferrocenes: Homogenous Catalysis, Organic Synthesis, Materials Science* (Eds.: A. Togni, T. Hayashi), Wiley-VCH, Weinheim, **1995**, Chapter 8, and references therein.

[5] a) H. Schottenberger, K. Wurst, U. J. Greisser, R. K. R. Jetti, G. Laus, R. H. Herber, I. Nowik, *J. Am. Chem. Soc.* **2005**, *127*, 6795; b) D. Braga, F. Grepioni, *Chem. Soc. Rev.* **2000**, *29*, 229; c) R. J. Webb, M. D. Lowery, Y. Shiomi, M. Sorai, R. J. Wittebort, D. N. Hendrickson, *Inorg. Chem.* **1992**, *31*, 5211; d) J.-F. Bérar, B. Calvarin, D. Weigel, *J. Chem. Phys.* **1980**, *73*, 438.

[6] a) C. Faulmann, P. Cassoux, *Prog. Inorg. Chem.* **2003**, *52*, 399, and references therein; b) C. L. Beswick, J. M. Schulman, E. I. Stiefel, *Prog. Inorg. Chem.* **2003**, *52*, 55, and references therein; c) S. Alvarez, R. Vicente, R. Hoffmann, *J. Am. Chem. Soc.* **1985**, *107*, 6253.

[7] a) A. T. Coomber, D. Beljonne, R. H. Friend, J. L. Brédas, A. Charlton, N. Robertson, A. E. Underhill, M. Kurmoo, P. Day, *Nature* **1996**, *380*, 144; b) J. Nishijo, E. Ogura, J. Yamaura, A. Miyazaki, T. Enoki, T. Takano, Y. Kuwatani, M. Iyoda, *Solid State Commun.* **2000**, *116*, 661; c) M. Uruichi, K. Yakushi, Y. Yamashita, J. Qin, *J. Mater. Chem.* **1998**, *8*, 141; d) H. Nakajima, M. Katsuhara, M. Ashizawa, T. Kawamoto, T. Mori, *Inorg. Chem.* **2004**, *43*, 6075; e) X. Ren, Y. Chen, C. He, S. Gao, *J. Chem. Soc., Dalton Trans.* **2002**, 3915.

[8] Z. Ni, X. Ren, J. Ma, J. Xie, C. Ni, Z. Chen, Q. Meng, *J. Am. Chem. Soc.* **2005**, *127*, 14330, and references therein.

[9] a) M. Almeida, R. T. Henriques, in *Handbook of Organic Conductive Molecules and Polymers* (Ed.: H. S. Nalwa), Wiley, New York, **1997**, p. 87; b) G. R. Lewis, I. Dance, *J. Chem. Soc., Dalton Trans.* **2000**, 3176.

[10] a) R. Kato, T. Imakubo, H. Yamamoto, R. Maeda, M. Fujiwara, J. Yamaura, H. Sawa, *Mol. Cryst. Liq. Cryst.* **2002**, *380*, 61; b) H. M. Yamamoto, J.-I. Yamaura, R. Kato, *J. Am. Chem. Soc.* **1998**, *120*, 5905; c) T. Imakubo, H. Sawa, R. Kato, *J. Chem. Soc. Chem. Commun.* **1995**, 1097.

[11] T. Mochida, K. Takazawa, M. Takahashi, M. Takeda, Y. Nishio, M. Sato, K. Kajita, H. Mori, *Inorg. Chem.* **2005**, *44*, 8628.

[12] a) T. Mochida, K. Takazawa, M. Takahashi, M. Takeda, Y. Nishio, M. Sato, K. Kajita, H. Mori, M. M. Matsushita, T. Sugawara, *J. Phys. Soc. Jpn.* **2005**, *74*, 2214; b) T. Mochida, S. Yamazaki, S. Suzuki, S. Shimizu, H. Mori, *Bull. Chem. Soc. Jpn.* **2003**, *76*, 2321; c) T. Mochida, *Mol. Cryst. Liq. Cryst.* **2000**, *343*, 205.

[13] a) J. S. Miller, J. C. Calabrese, A. J. Epstein, *Inorg. Chem.* **1989**, *28*, 4230; b) A. E. Pullen, C. Faulmann, I. I. Pokhodnya, P. Cassoux, M. Tokumoto, *Inorg. Chem.* **1998**, *37*, 6714; c) M. Fettouhi, L. Ouahab, M. Hagiwara, E. Codjovi, O. Kahn, H. Constant-Machado, F. Varret, *Inorg. Chem.* **1995**, *34*, 4152; d) M. W. Day, J. Qin, C. Yang, *Acta Crystallogr. Sect. C* **1998**, *54*, 1413; e) S. Zürcher, J. Petrig, M. Perseghini, V. Gramlich, M. Wörle, A. Togni, *Helv. Chim. Acta* **1999**, *82*, 1324; f) S. Zürcher, V. Gramlich, D. Arx, A. Togni, *Inorg. Chem.* **1998**, *37*, 4015; g) M. Hobi, S. Zürcher, V. Gramlich, U. Burckhardt, C. Mensing, M. Spahr, A. Togni, *Organometallics* **1996**,

15, 5342; h) V. Da Gama, D. Belo, I. C. Santos, R. T. Henriques, *Mol. Cryst. Liq. Cryst. Sci. Technol., Sect. A* **1997**, *306*, 17.
[14] D. Bellamy, N. G. Connelly, R. G. Lewis, A. G. Orpen, *CrystEngComm* **2002**, *4*, 51.
[15] N. J. Mammano, A. Zalkin, A. Landers, A. L. Rheingold, *Inorg. Chem.* **1977**, *16*, 297.
[16] T. Mochida, S. Suzuki, H. Moriyama, H. Terao, T. Sugawara, *Acta Crystallogr. Sect. C* **2000**, *56*, 1183.
[17] S. P. Best, S. A. Ciniawsky, R. J. H. Clark, R. C. S. McQueen, *J. Chem. Soc., Dalton Trans.* **1993**, 2267.
[18] T. Mochida, T. Akasaka, Y. Nishio, K. Kajita, H. Mori, unpublished results.
[19] a) K.-F. Tebbe, R. Buchem, *Z. Kristallogr.* **1996**, *211*, 689; b) T.-Y. Dong, H.-M. Ling, M. -Y, Hwang, T.-Y. Lee, L.-H. Tseng, S.-M. Peng, G.-H. Lee, *J. Organomet. Chem.* **1991**, *414*, 227.
[20] a) D. N. Hendrickson, Y. S. Shon, H. B. Gray, *Inorg. Chem.* **1971**, *10*, 1559; b) B. N. Figgis, M. Gerloch, R. Mason, *Proc. R. Soc. London Ser. A* **1969**, *309*, 91.
[21] J. S. Miller, D. T. Glatzhofer, C. Vazquez, R. S. McLean, J. C. Calabrese, W. J. Marshall, J. W. Raebiger, *Inorg. Chem.* **2001**, *40*, 2058.
[22] a) D. W. Allen, R. Berridghe, N. Bricklebank, S. D. Forder, F. Palacio, S. J. Coles, M. B. Hursthouse, P. J. Skabara, *Inorg. Chem.* **2003**, *42*, 3975; b) D. Braga, M. Eckert, M. Fraccastoro, L. Maini, F. Grepioni, A. Caneschi, R. Sessori, *New J. Chem.* **2002**, *26*, 1280.
[23] T. Mori, A. Kobayashi, Y. Sasaki, H. Kobayashi, G. Saito, H. Inokuchi, *Bull. Chem. Soc. Jpn.* **1984**, *57*, 627.
[24] Spartan '04, Wavefunction, Irvine, CA (USA), **2004**.
[25] a) A. L. Spec, *Acta Crystallogr. Sect. A* **1990**, *46*, C34; b) A. L. Spec, PLATON—A Multipurpose Crystallographic Tool, Utrecht University, Utrecht (The Netherlands), **2005**.
[26] G. M. Sheldrick, SHELXL, Program for the Solution of Crystal Structures, University of Göttingen, Göttingen (Germany), **1997**.
[27] ORTEP-3 for Windows: L. J. Farrugia, *J. Appl. Crystallogr.* **1997**, *30*, 565.

Received: September 5, 2006
Published online: November 30, 2006

